IEEE Access
Multidisciplinary : Rapid Review : Open Access Journal

Received 7 November 2022, accepted 21 November 2022, date of publication 28 November 2022, date of current version 2 December 2022.

Digital Object Identifier 10.1109/ACCESS.2022.3225098

RESEARCH ARTICLE

Magnetoelectric Nanoparticles: Evaluating Stimulation Feasibility of the Possible Next Generation Approach for Deep Brain Stimulation

EMMA CHIARAMELLO, (Member, IEEE), SERENA FIOCCHI, MARTA BONATO, (Student Member, IEEE), ALESSANDRA MARRELLA, GIULIA SUARATO, MARTA PARAZZINI, (Member, IEEE), AND PAOLO RAVAZZANI, (Member, IEEE)

Istituto di Elettronica e di Ingegneria dell'Informazione e delle Telecomunicazioni, Consiglio Nazionale delle Ricerche, 10129 Turin, Italy

Corresponding author: Emma Chiaramello (emma.chiaramello@cnr.it)

ABSTRACT The purpose of this study is to quantify the distributions of the electric field induced by $CoFe_2O_4$ core - $BaTiO_3$ shell magneto-electric nanoparticles (MENPs) when localized in deep brain structures. These fields can be used for deep brain stimulation (DBS), and their effect is compared to the fields induced by conventional DBS electrodes in monopolar and bipolar configuration. A computational approach based on finite element method was applied, along with the use of a highly detailed anatomical model of the brain structures. Different MENPs configurations were investigated and compared to conventional DBS electrode configuration. The activation of nervous fibers was quantified by calculating the Activation Function (AF) defined as the second derivative of the electric potential along the fiber. Electric field amplitudes obtained by MENPs were much lower than the ones obtained by the monopolar and bipolar electrode configurations. The AF values showed that MENPs were able to obtain very localized activation patterns along the fibers. In addition to the minimal invasiveness and proven biocompatibility of the MENPs, the results show that the proposed approach represents an important step towards a selective and minimally invasive strategy for DBS. All these findings are essential in identifying the unique characteristics that MENPs could provide for nervous system stimulation, and how the use of MENPs could improve the development of a new generation of DBS techniques.

INDEX TERMS Activation function, deep brain stimulation, magneto-electric nanoparticles, minimally invasive approach, nanotechnology.

I. INTRODUCTION

Alterations in neurological functions due to different causes (e.g., stroke, trauma, neurodegeneration, epilepsy, neuropsychiatric diseases, among others) commonly exhibits alterations in brain rhythms and activity patterns. This is translated in a need of increasingly more efficient strategies of neural stimulation and controlling of neural activity. One of the well-established neurostimulation techniques successful in reducing symptoms in different neurological disorders, as Parkinson's disease [1], essential tremor [2], and epilepsy [3], [4] is Deep Brain Stimulation (DBS) (see, e.g. [5] and [6]). DBS consists in using electrodes implanted by stereotactic neurosurgical techniques in the deep regions of the brain [7], to stimulate basal ganglia using trains of electric biphasic (or, more rarely, monophasic) pulses with a main frequency in the range 120-180 Hz. Clinical benefits of DBS are largely dependent on the spatial distribution of the stimulation field in relation to brain anatomy [8], [9], [10], [11], maximizing the beneficial effects on motor symptoms if the electric stimulation is localized in the subthalamic nucleus (STN). STN is a small nucleus responsible for body

The associate editor coordinating the review of this manuscript and approving it for publication was Larbi Boubchir.

This work is licensed under a Creative Commons Attribution 4.0 License. For more information, see https://creativecommons.org/licenses/by/4.0/

movements and coordination, mainly connected to another structure known as globus pallidus (GP), which carries output to the thalamus (Th) [12], [13]. All these structures form the anatomical nuclei of the basal ganglia and are located among the deep structures of the brain.

Although the quality of life of patients is largely improved by DBS, it remains a highly invasive procedure. Despite the efforts towards less invasive and safer surgical procedures, smaller and longer-lasting devices, DBS presents drawbacks such as hemorrhages, infections, skin erosions, malfunction of the cables, or reaction of the tissue that prevents the electrode's function [14], [15]. This makes the development of new generation technologies for neural stimulation essential to allow a wider use of DBS.

An encouraging approach for neural tissue stimulation is offered by ad hoc engineered nanoparticles [16]. Among the different types of materials, magneto electric nanoparticles (MENPs) are very promising, as, due to their multiferroic structure, made of a ferromagnetic core and ferroelectric shell, they exhibit the so-called magneto electric (ME) effect, i.e. the capability of generating a high amplitude electric field when stimulated by a small amplitude magnetic field [17], [18]. This characteristic, along with their tested biocompatibility (see, e.g., [19] and [20]), allows MENPs being promising tools in all the biomedical fields requiring an interaction between electric field and biological tissues. An important aspect that makes MENPs being so promising for neural tissue stimulation, and in particular for DBS, is their minimum invasiveness: even if the MENPs need to be inserted into brain structures and the delivery methods already experimented in *in-vivo* animal studies include stereotactic [19] and intravenous [20] injections, i.e. invasive approaches, the possibility of using nano-scale devices with proven biocompatibility could represent a disruptive step ahead in term of ''long-term invasiveness'' if compared with current DBS techniques [21]. Some recent in vivo studies analyzed the feasibility of using MENPs for central nervous system stimulation: in [22], the authors injected intravenously core-shell CoFe2O4-BaTiO3 MENPs forcing them to cross the blood-brain barrier and localizing them to the brain target by applying a static magnetic field. MENPs were then activated by a low amplitude magnetic field (below 1000 Oe or 80 kA/m) to induce a local electric field (on the order of 1000 V/m) due to the magnetoelectric effect. In [23] the same authors analyzed the capability of MENPs to modulate brain in vivo when stimulated with a 100 Oe (equal to 8 kA/m) magnetic field in the 0 - 20 Hz frequency range. Results of a more recent study [20] showed a cortical activation of individual neuron and large neural networks in vivo by activating MEPNs with a pair of electromagnets at about 350-450 Oe (equal to 28-36 kA/m).

An interesting and recent experimental proof of concept of the use of MENPs in DBS was proposed in [19]: by means of stereotactic injection, MENPs were placed into the subthalamic region of mice and stimulated by coupling DC and 140 Hz AC magnetic fields, with amplitude equal to 220 and 6 mT, respectively. After 7 weeks, nanoparticles were found to be still localized in the target area, and results showed that MENPs induced neural activity able to activate regions of the cortico basal ganglia-thalamocortical circuit, thus indicating the approach as feasible for a wireless activated stimulation in DBS.

Along with these very encouraging experimental results, an in-silico characterization based on computational modeling of the electric quantities involved when using MENPs for DBS and their correlation with neural activation is essential. Computational methods represent unique tools for a better understanding of the insights under phenomena of interest in neural stimulation, and indispensable enablers of translation towards clinical use of new stimulation approaches. However, except than for our recent study [24], in which the use of MENPs for stimulation of cortical and subcortical areas was investigated in terms of electric field distribution and the tissue penetration by computational modeling, no previous study modeled and quantified electric quantities involved in the use of MENPs for neural stimulation, especially regarding their use for DBS.

This study aims at filling this research gap, by using computational models to quantify the distributions of the electric field and electric potential induced by CoFe2O4 core - BaTiO3 shell MENPs when localized in the STN structures in a highly detailed anatomical head model, and by numerically comparing them to the distributions obtained by conventional DBS monopolar and bipolar electrode configurations. Following the approach described by [25], the activation function AF, defined as the second space derivative of the electric potential along a fiber direction and usually considered as indicative of excitation or inhibition of neuronal fibers, was calculated along 30 fibers connecting the STN to the GP considering different MENPs configurations. At this stage, the evaluation of AF allows obtaining a first evaluation of the excitation or inhibition of neuronal fibers. Even if a more quantitative evaluation of the response of the fibers obtained by coupling the dosimetric model to biophysical models of neurons (see, e.g. [9] and [26]) is beyond the scope of this study, comparing AF behaviors obtained by various MENPs configurations to the AF thresholds described in literature will provide important information for the comprehension of a MENPs-based DBS. All these findings will be essential in identifying the unique characteristics that MENPs could provide for nervous system stimulation, and how the use of MENPs could improve the development of a new generation of DBS techniques.

II. MATERIALS AND METHODS

A finite element method (FEM) as implemented in the simulation platform Sim4Life (by ZMT Zurich Med Tech AG, Zurich, Switzerland, www.zurichmedtech.com) was used in this study, following a methodology described in previous publications [27], [28] and detailed here below.

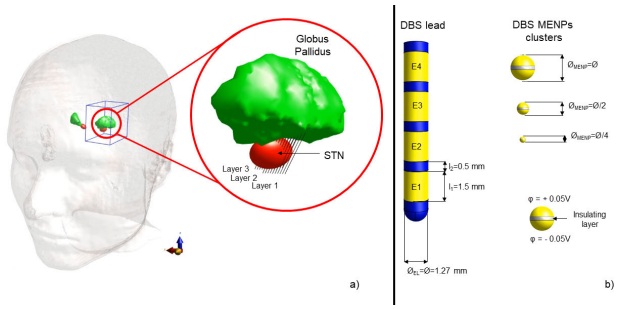

FIGURE 1. (a) Anatomical model MIDA and detail of the STN (red tissue), the globus pallidus (green tissue) and the 3 parallel layers, each made of 10 fibers, going from the STN to the GP. (b) Schematic view of the DBS electrode and the MENPs clusters.

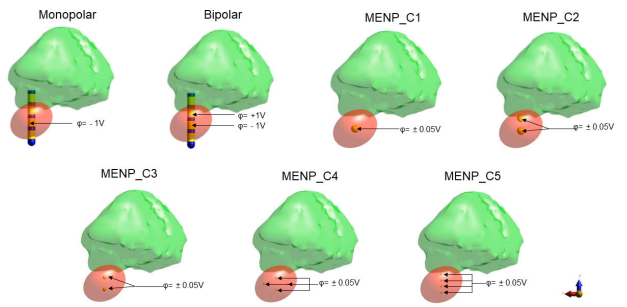

FIGURE 2. Schematic view of the electrode, in both monopolar and bipolar configurations, and the MENPs clusters in the various configurations, localized in STN structure (red tissue). The green tissue represents the GP.

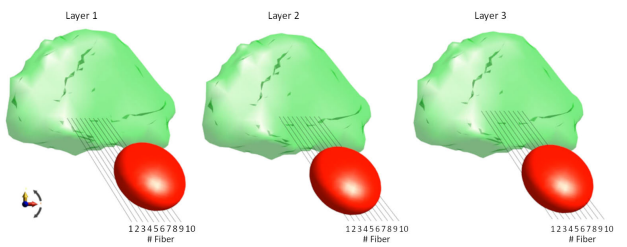

FIGURE 3. Schematic representation of the geometrical configurations of the three layers of fibers, each composed by 10 parallel fibers ordered from 1 to 10 and going from the STN structure (red tissue) to the GP (green tissue).

A. ANATOMICAL MODEL

A multimodal imaging-based detailed anatomical model [29], of the human head and neck, named "MIDA" was imported in the simulation platform Sim4Life. The model was segmented and reconstructed at an isotropic resolution equal to 0.5 mm, which allowed to distinguish the tissues mainly involved in the DBS stimulation protocols, such as globus pallidus (GP), white matter, thalamus and subthalamic nuclei (STN). Since this last tissue, which is the main target of the stimulation, was not segmented in the original MIDA model, we performed a manual segmentation of this structure by comparing the STN position, orientation and dimension with MR images-based brain atlas and literature data [30], [31], [32], [33], [34]. The resulting STN nuclei have an ellipsoidal shape with a volume equal to $6 \times 8 \times 9$ mm^3 (width x length x diameter), main axis directed 60 degrees from the horizontal plane of the anterior commissure-posterior commissure line (AC-PC) and 20 degrees from the sagittal plane, and centre at x= $\pm$11mm (lateral), y = -3 mm (posterior), z = -4 mm (inferior) from the midcommissural point (Fig 1a).

Since neural activity between subthalamic nucleus and internal GP is severely impaired in Parkinson Disease (PD), we also modelled 3 parallel layers of 10 fibers for each layer (direction along the main STN axis, equally spaced with a step of 0.5 mm along the antero-posterior direction, and inter-layers distance equal to 1 mm) connecting these structures on the right hemisphere, where we focused our analysis under the hypothesis of symmetry between the two hemispheres. Each fiber has a length of 14 mm, going from the STN to the GP. When describing the position along each fiber's length, position 0 was defined as corresponding to the initial point of the fiber, in vicinity of the STN tissue, while position 14 mm was at the end of the fiber, in proximity of the GP. The geometrical characteristics of the three layers, their reciprocal position and the numerical labels corresponding to each fiber are represented in fig. 3.

B. ELECTRODE AND MENP CLUSTER MODELING

To simulate MENPs as sources for DBS, they were modeled as spherical agglomerates of diameter comparable to the classical DBS electrodes' (i.e. Ø=1.27 mm), in accordance with experimental procedure and findings described in [19]. MENPs clusters were placed in STN considering five configurations using different dimensions and locations of the MENPs (see Fig. 2):

1) "MENP_C1": one MENPs cluster, of diameter equal to Ø, positioned in the center of the STN.
2) "MENP_C2": two MENPs clusters, each of diameter equal to Ø, positioned in correspondence of the positions in which the active contacts E1 and E2 of the classical DBS electrode (see Fig.1b) would be placed.
3) "MENP_C3": two MENPs clusters, each of diameter equal to Ø/2, in correspondence of the positions in which the active contacts E1 and E2 of the classical DBS electrode would be placed.
4) "MENP_C4": four MENPs clusters, each of diameter equal to Ø/4, two of which positioned as in the previous configuration, the other two in the same plane, at a distance of 2 mm from the first two, to avoid reciprocal influence.
5) "MENP_C5": four MENPs clusters, each of diameter equal to Ø/4, positioned aligned in the vertical direction at a distance of 1 mm from each other.

Due to their core and shell chemical compositions, MENPs are characterized by strong coupling between magnetic and electric fields, the so-called magneto-electric (ME) effect, quantified by the magneto-electric coefficient α:

$$\alpha = \Delta P_i / \Delta H_i, \tag{1}$$

where P_i is induced electric polarization, and H_i is the applied magnetic field. The electric potential on each MENP surface was found to exhibit a dipole distribution [35], [36] aligned along the direction of the low-amplitude magnetic field used for stimulating the ME effect. When considering a great number of MENPs, such as in the spherical agglomerates modelled in this study, the macroscopic behavior could be approximated following different approaches. In this study, hypothesizing that all the MENPs could be approximated by dipoles orientated along the same direction, and with the same potential of their surfaces, we modeled the distribution of the electric potential on the MENPs agglomerates by dividing the surface of the spheres in two areas, one characterized by positive potential and one by a negative one, divided by an insulating layer (see fig.1b). This approach, which is the same regardless to the cluster dimension, is reasonable following the approximation of electric potential on the surface of a volume containing electric sources modeled as dipoles, using the definition of "volume dipole moment density function" as detailed in [37]. For all the considered MENPs configurations, the amplitude of the electric potential on each MENPs cluster was set equal to $\varphi = \pm 0.05$ V, a reasonable value considering the experimental values observed in previous studies (see, e.g. [19], [23] and [35]). For all MENPs configurations a potential equal to 0 V was set at the boundaries of the computational domain, containing all the MIDA tissues (size = 216.6 × 162.6 × 232.5 mm^3).

As a comparison, the distal end of a traditional DBS lead (Medtronic 3389) was modelled and inserted perpendicular to the transversal plane of the model with the center of the 2nd contact from the bottom coincident to the center of the subthalamic nucleus. The portion of the lead modelled, consists of 4 cylindrical conductive contacts (1.5 mm in height, 1.27 mm in external diameter, 0.96 in internal diameter) with 0.5 fully insulated inter-electrode spacing (Fig 1b). The conductive contacts (represented in yellow in Fig 1b) were modelled as perfect electric conductors (PEC), whereas the insulated sections (represented in blue in Fig.1b) as polyurethane (electrical conductivity $\sigma = 0$ S/m, relative electrical permittivity εr =3.4).

The following electrodes configurations were implemented (see Fig. 2):

1) "Monopolar" configuration: contact E2 was set as active to a voltage-controlled boundary condition (Dirchlet boundary condition set to φ =-1 V), the return electrode ($\varphi = 0$ V) was represented using the boundary of the computational domain (size = 216.6 × 162.6 × 232.5 mm^3). This configuration, even if hardly used in current DBS systems, has been simulated for the sake of comparison with "MENP C1" configuration.
2) "Bipolar" configuration: contact E2 and E3 were set to voltage-controlled boundary conditions at −1 V and + 1 V, respectively.

Sinusoids at a frequency of 130 Hz, similar to the typical repetition frequency used in DBS applications [38], [39] were administered to both electrodes and MENPs clusters.

C. ELECTRODE AND MENP CLUSTER MODELING

In this frequency range the electromagnetic ohmic quasi-static approximation applies and it was used to solve the Laplace equation:

$$\nabla \cdot (\sigma \nabla \varphi) = 0, \tag{2}$$

where φ is the electric potential, σ (S/m) is the electrical conductivity of tissues set according to the DBS frequency [40]. The electric field (**E**) distribution in all the model tissues was then obtained by means of the following relation:

$$\mathbf{E} = -\nabla \varphi \tag{3}$$

A rectilinear uniform rectilinear mesh with a 0.1 mm maximum step was used to discretize the region around the STN and GP, and 1 mm step size elsewhere, resulting in about 90 million elements total.

From the potential distribution, we calculated the Activating Function (AF) defined as the second space derivative of φ, along the fibers lenght:

$$AF\,(x) = \partial^2 \varphi(x)/\partial x^2 \tag{4}$$

AF provides a quantitative measure of the excitation/inhibition of each fiber [25].

III. RESULTS

Fig. 4 shows, as an example, the E field distributions in the STN obtained for the MENP_C1 configuration, and, as a comparison, for monopolar and bipolar electrodes configurations. As a general observation, the E field distributions due to the presence of MENPs appear well localized around the cluster of nanoparticles, while for the electrodes the E field distributions are more widespread in the tissues: even if the dimensions of the sources (MENPs and active contact) and stimulation approaches were identical, the shape of the distribution was different, probably due to the presence of conductive, although as non-active, components of the electrode. Table 1 shows the 99th percentiles and the median values of the root mean square (RMS) of the E field induced in the STN: values were found to be very similar across the MENPs configurations. As a comparison, 99th percentiles and the median values of the E field distributions induced in the STN by the electrode in monopolar and bipolar configurations were ten/twenty times higher - due to the ten/twenty times higher surface potentials fixed on the active contacts.

Fig. 5 shows, as an example, the electric potential φ (fig. 5a and c) along one of the fibers modelling the nervous connection between the STN and the GP and the corresponding AF (fig. 5b and d) for the MENP_C1 and the electrode monopolar and bipolar configurations. As well expected, due to the difference in the boundary conditions on the MENPs cluster and the active contact of the electrodes (φ equal to ±0.05 V for MENPs configuration, equal to 1 V for monopolar configuration and to ±1 V for bipolar configuration), the electric potential along the fibers for the MENP_C1 configuration is ten/twenty times lower than that observed for the monopolar and bipolar electrodes, respectively. When considering AF for MENP_C1 slightly positive values were

observed between 5 and 7.5 mm along the fiber, followed by negative values, i.e. inhibitory effect, between 7.5 and 9 mm along the fiber, and positive values, i.e. excitatory effect, between 9 and 10 mm. A very similar behavior, with alternating inhibitory and excitatory effects, was observed for the bipolar electrode configuration, while a slightly different behavior was observed for the monopolar electrode configuration. For this latter, negative values were observed between 3 and 7.5 mm along the fiber, positive values, i.e. excitatory effect, between 7.5 and 10 mm, and again negative until the end of the fiber. Maximum AF values were equal to 6.0 x10^4, 3.3 x 10^5 and 7.5 x 10^5 V/m^2, localized at 9.5, 8.8 and 8.7 mm along the fiber, for MENP_C1, monopolar and bipolar electrode configurations, respectively.

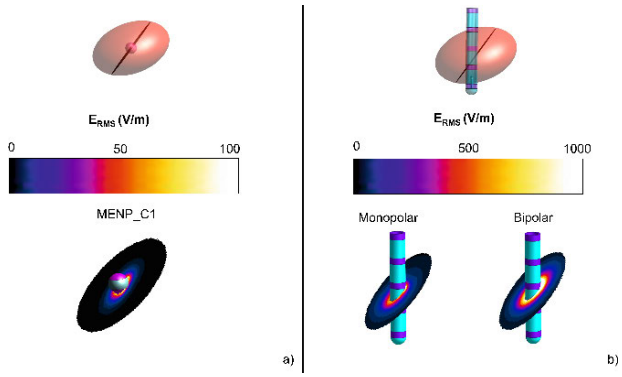

FIGURE 4. RMS E field distributions on a transversal plane passing in the center of the STN obtained for the MENP_C1 configuration (a), and for the monopolar and bipolar electrodes configurations (b).

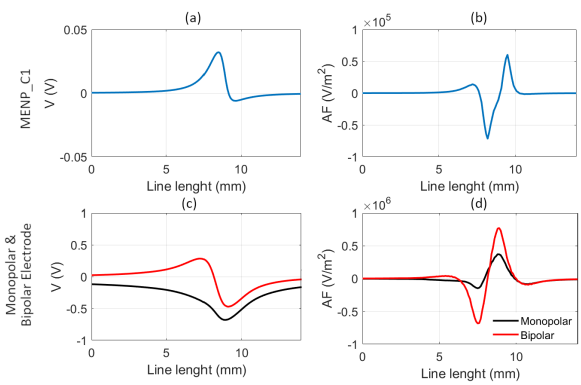

FIGURE 5. Electric potential φ and its second derivate AF along the fiber #8 of layer 1 for the MENP_C1 (first row) and monopolar electrode (second row) configurations.

Table 1 shows the descriptive statistic of AF values in terms of maximum and minimum values. For all the MENPs configurations, except than for MENP_C1 in which results showed AF values in the range of ±1.5 x 10^5 V/m^2, the maximum and minimum AF values were of the order of magnitude of ±10^6 V/m^2. These values were similar to the results obtained with the electrode configurations, in particular for the monopolar case.

Fig. 6 and fig. 7 show, for each of the ten fibers in each layer (namely #1, #2, #3, as defined in fig. 1), the AF obtained

TABLE 1. Descriptive statistics of E field and AF values.

	E_{RMS} in STN (V/m)		AF (V/m^2)	
	99th perc	Median	min	max
MENP_C1	78	2	-1.5*10^5	1.5*10^5
MENP_C2	118	2	-1.6*10^6	1.5*10^6
MENP_C3	118	1	-1.5*10^6	1.5*10^6
MENP_C4	92	1	-1.2*10^6	1.2*10^6
MENP_C5	108	0.6	-1.5*10^6	1.5*10^6
Monopolar	901	96	-1.2*10^6	1.6*10^6
Bipolar	1871	112	-2.8*10^6	3.1*10^6

for each MENPs (fig. 6) and for the monopolar and bipolar electrode configurations (fig. 7). To compare the distributions of the AF along the fibers for MENPs and electrode configurations, the maximum value of the colormap is fixed equal to $AF^{Th}_{mean} = 5 \times 10^4$ V/m^2. This value was chosen as a medium threshold among the AF thresholds identified by Duffley et al. [26] as sufficient to cause nervous fiber activation, considering different electrodes configurations and 5.7 μm diameter mammalian motor axons [41]. AF^{Th}_{mean} value thus represents a rough indication of the AF threshold for the activation of a myelinated nervous fiber. As a first observation, for all the MENPs configurations the maximum values of AF were found along the fibers of the layer #2, while for layers 1 and 3 the AF was found to reach values higher or comparable to AF^{Th}_{mean} only in few fibers. When observing a single fiber, AF values different from zero were focused along a small portion of the fiber length, alternating negative and positive values.

For MENP_C1 in layer 1 the AF values showed values comparable to AF^{Th}_{mean} only for fiber from 1 to 3, while in layer 2 fibers 2 to 8 showed values higher than 4×10^4 V/m^2 and in layer 3 fibers 1 to 5 showed values higher than 4×10^4 V/m^2. For MENP_C2, i.e., when inserting a second MENPs cluster with the same dimensions, no remarkable difference in the AF was noticed, except than for the shape obtained along the fibers 1 to 6 of the layer 3, that reflected the presence of two sources. For MENP_C3, i.e., when considering two clusters placed in the same positions of MENP_C2 configurations, but with smaller dimensions, the patterns of AF values along fibers showed different shapes compared to the ones observed for MENP_C1 and MENP_C2. Layers 1 and 3 showed similar patterns, with smaller AF values compared to those observed for the same layers in MENP_C1 and MENP_C2. The highest AF values were found along layer 2, with fibers from 2 to 8 showed maximum AF values comparable or higher than AF^{Th}_{mean}. For MENP_C4 configuration, i.e., when considering 4 MENPs clusters with diameter equal to Ø/4, layer 1 showed AF values higher or comparable to AF^{Th}_{mean} along fibers 3 to 5. For layer 2, AF values were more focused along fibers than in the other MENPs configuration, with values higher than AF^{Th}_{mean} along fibers 3 and 4, at a position of 0.7 mm, and along fibers 6 and 7, at a position of 0.5 mm. Finally, for MENP_C5 configuration, i.e. when considering 4 MENPs clusters with the same dimensions of MENP_C4, but aligned along the

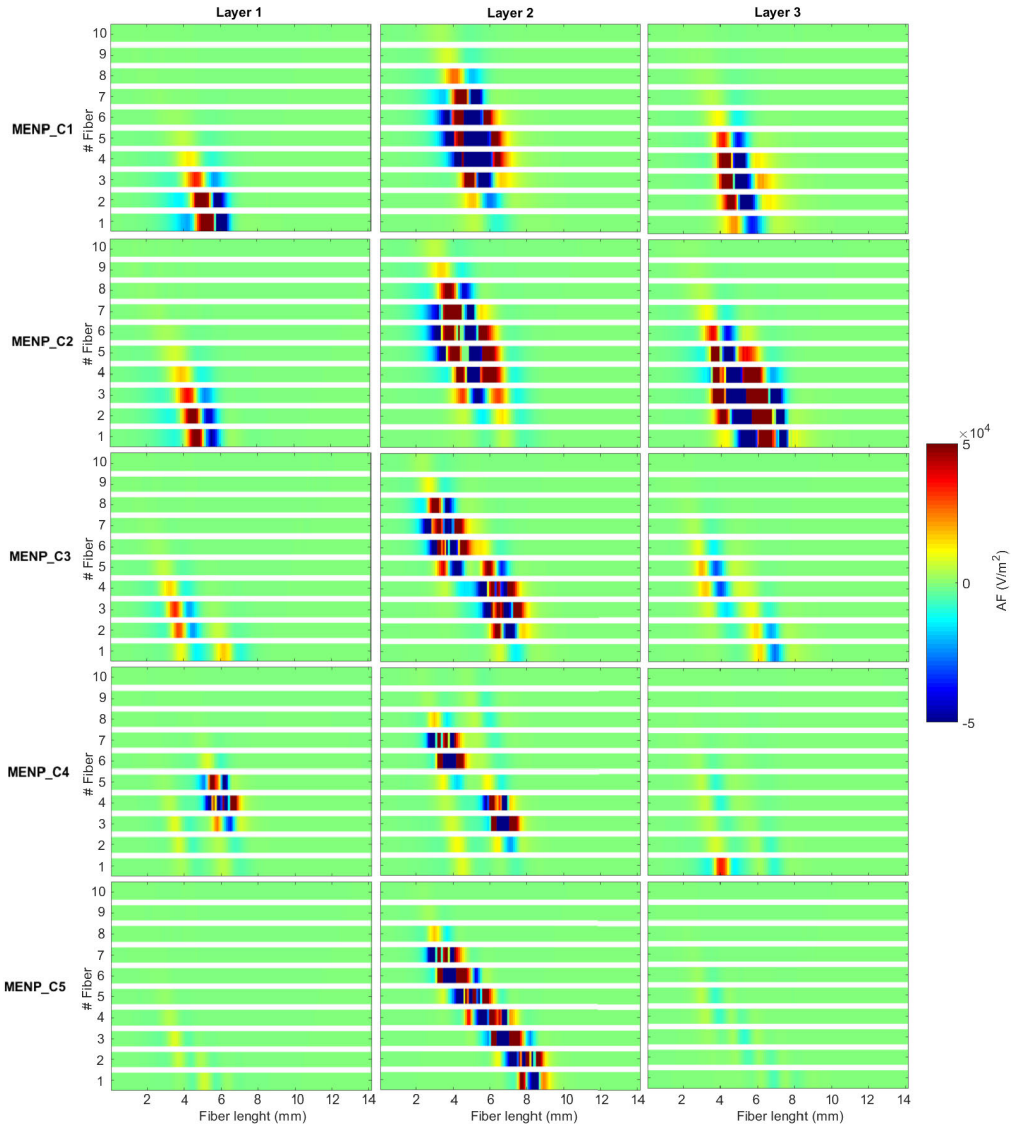

FIGURE 6. AF values obtained along the ten fibers of each layer (columns) for each MENPs configuration (rows).

vertical direction, AF showed negligible values for the fibers in layers 1 and 3, while almost all the fibers of layer 2 showed AF values higher than AF^{Th}_{mean}.

As to the AF values obtained by the electrode in monopolar and bipolar configurations (fig. 7), results indicates that almost all the fibers in all the considered layers showed AF values comparable or higher than AF^{Th}_{mean}. AF showed non-zero values for almost all the fibers' length, alternating negative and positive values.

Fig. 8 shows the quantification of the percentage of length of each fiber, summarized by layers, for which the obtained AF values were higher or equal to AF^{Th}_{mean}, i.e. the percentage of points along the fibers that could represent a starting point for action potential. For MENP configurations these percentages were found to be lower than 4% in all cases, much below those observed in monopolar and bipolar electrodes configurations. For MENP_C3 and MENP_C5 percentages equal to 2.4 and 2.9%, respectively, were found along layer 2, while in the other layers the percentage was equal to zero. For MENP_C1 and MENP_C4 the higher percentage, equal to 2.5 and 1.4 respectively, were found for layer 2, while a small percentage, lower than 1% was found for the fibers belonging to layer 1 and 2. MENP_C2 showed the highest percentages, equal to 3.9 and 3.1 % for layer 3 and 2, respectively. On the contrary, for the traditional electrodes the percentages of length of each fiber for which AF was higher than AF^{Th}_{mean} were much higher, with minimum values equal to 6.5 and 7.7% along layer 1 for monopolar and bipolar configuration respectively, and maximum values equal to 10.1% along layer 2 for monopolar and 15.2% along layer 3 for bipolar configurations. These results showed that MENPs allowed focusing the activation on specific areas of the nervous fibers with great selectivity among layers.

IV. DISCUSSION

In the context of the growing interest for new approaches for minimizing invasiveness while maximizing efficiency and spatial accuracy of brain stimulation MENPs could play a

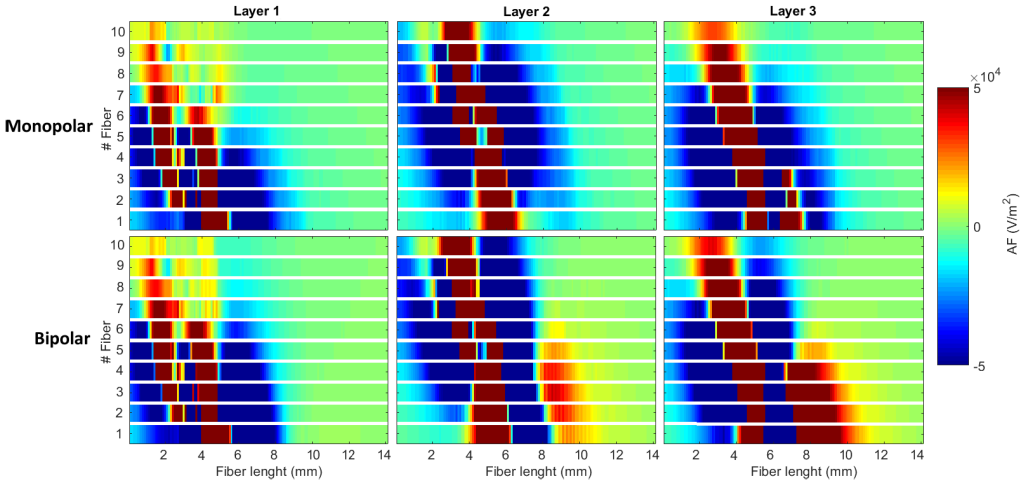

FIGURE 7. AF values obtained along the ten fibers of each layer (columns) monopolar (first row) and bipolar (second row) electrode configuration.

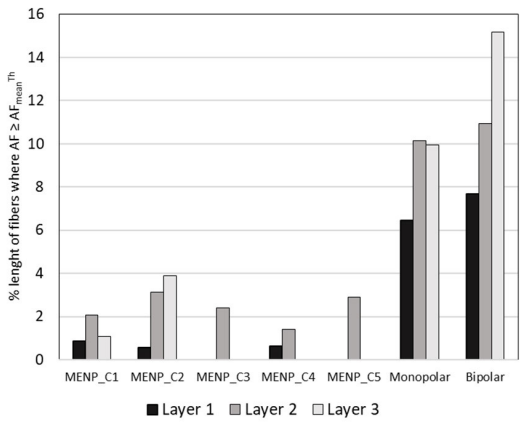

FIGURE 8. Percentage of length of each fiber, summarized by layers, for which the obtained AF values were higher or equal to AF^{Th}_{mean}, for MENPs configurations, and, as a comparison, for the conventional monopolar and bipolar electrodes configurations. Note that the difference in the percentages between MENPs and electrodes configurations reflects the difference in the potential amplitudes between the two approaches.

fundamental role. In this study the feasibility of using MENPs as minimally invasive sources, if compared with conventional electrodes, for DBS was investigated. A computational approach was used to quantify the distributions of the E fields induced by $CoFe_2O_4$-$BaTiO_3$ MENPs placed in STN with different configurations, and results were compared to those obtained by conventional DBS monopolar and bipolar electrode configurations.

The E field distributions due to the presence of MENPs appeared as well localized around the clusters of nanoparticles, while for the electrodes, the E field distributions were more widespread in the tissues. This difference was probably not due to the slightly different geometry between the spherical cluster of MENPs and the active contact, but to the presence in the electrode of other conductive, although as non-active, components of the electrode, that could influence the electric field distribution [42]. As to the amplitude of the E field induced by MENPs, the presence of different number of MENPs was found to be minimally influential on the 99th percentile and the median value of the distribution. As well expected, the amplitude of the E field induced by MENPs was ten/twenty times lower than the amplitude induced by the electrode in monopolar and bipolar configurations, respectively. This was due to the amplitude of the electric potential set on the surface of each MENPs cluster, ten/twenty times lower to the potential set on the active contacts in monopolar/bipolar electrode configurations. The choice of using such a value was based on previous experimental characterization of different types of MENPs, as the characterization of a specific MENP is beyond the scope of the study. In [43] the ME coefficient in different $CoFe_2O_4$ core - $BaTiO_3$ shell MENPs has been measured to be in the range from 10 to over 100 mV cm^{-1} Oe^{-1}, corresponding to 10-100 kV m^{-1} T^{-1}. In [35] the authors found a surface potential almost equal to 40 mV, with a dipole distribution aligned to the external magnetic field on the surface of a 80 nm MENP when stimulated by a 60 Hz magnetic field at 5 mT. Considering these measurements, and hypothesizing that the high number of MENPs in each of the spherical agglomerate modelled in this study would be aligned all in the same direction, i.e. the one of the external magnetic field, an amplitude of 100 mV, corresponding to the ±50 mV values set of the two parts of the surface of the each agglomerate, that would correspond to a stimulating AC magnetic field of amplitude 12.5 mT if using the same MENPs described in [35], appeared reasonable. This value is widely achievable with conventional coils systems, such as Helmhotz coils (e.g., R=20 cm, NxI= 3000 A, uniform B between the two Helmholtz coils = 13.5 mT) or a simple TMS circular coil (e.g., R= 5 cm, NxI= 10kA, B field in the center = 140 mT and Bfield at z=10 cm equal to 12.4 mT). Also more complex systems, such as deep TMS coils, which allow to reduce the rapid decay of B-field with distance, could be eventually used to elicit the magnetoelectric behavior. Using these more complex systems could allow obtaining amplitude of the B field at the subthalamic level even 50 times stronger than the ones required by our assumptions (see e.g., [44]). Of course, a detailed set of simulations of realistic systems for eliciting MENPS mediated stimulations

will be focus of in future studies to allow the technique to be translated into human applications. When considering AF, i.e., the second derivative of the electric potential along the fibers connecting the STN to the GP, results showed a similar behavior in terms of presence of inhibition and activation patterns for MENPs and monopolar/bipolar electrode configurations. The same fiber when stimulated with either MENPs or electrode may be excited in the region where the AF is positive and inhibited where the AF is negative. This finding agreed with results of previous studies [25], [45] reporting activation or inhibition of the fibers during the DBS stimulation. As to the amplitude of the AF, which can be a useful quantification of the response of the fibers, the values obtained by the MENPs configurations were lower than the values obtained by the electrodes. Many studies in literature focused on defining stimulation thresholds in terms of AF for DBS for different types and duration of stimuli, electrodes, stimulation protocols and axon dimensions: in [46] the authors found, using computational approach and axon cable models, that the mean AF threshold values for a 60 μs stimulus delivered by electrode similar to the one simulated here were equal to 3.62 x 10^5, 9.2 x 10^5 and 4.5 $\times$ 10^5 V/m^2 for axons with diameters equal to 2.5, 5 and 7.5 μm, respectively. In another study [47] the authors estimated the AF thresholds $\Delta^2 V/\Delta x^2$ for different stimulation configurations as being in the range 5-20, were Δx was equal to 5 mm. In [26] a wide range of DBS experimental conditions, including different types of electrodes, durations of stimuli and axon dimensions, were tested with the aim of defining AF thresholds and evaluating different strategies for estimating the activation volume. The authors showed AF thresholds within the range 2-8 $\times 10^5$ V/m^2. All these values were comparable to the AF values obtained by MENPs configurations in the present study, thus meaning that, even if the E field distributions obtained by MENPs were much lower than the ones obtained by the electrode, still an activation of nervous fibers occurred. Considering as a reference the AF threshold equal to 5 $\times$ 10^5 V/m^2, being a mean value across the conditions analyzed in [26], the activation patterns along the fibers for all the MENPs conditions were described. Results showed that MENPs were very accurate in stimulating precise fibers: even when considering the larger clusters, i.e., the ones with diameter equal to the diameter of the electrode active contacts, the AF function values higher than 5 $\times$ 10^5 V/m^2 were localized in small parts of the nervous fibers, while for both monopolar and bipolar electrode configurations almost all the considered fibers were activated. When simulating smaller MENPs clusters, the stimulation and activation patterns of the fibers were even more localized: only small percentages of the length of the analyzed fibers were activated, while elsewhere the AF values were almost equal to zero. These findings are very promising: in clinical practice it is known that accurate targeting of the correct brain structure is important for maximizing the clinical benefit of DBS therapy, despite the target structures are small, present non-spherical shapes and complex substructures [13], and are surrounded by other structures which upon stimulation can cause adverse side effects [39]. Due to their nanometric dimension, MENPs will allow very high spatial resolution in brain stimulation, including the possibility of targeting very precise and high detailed structures, such as GPi fibers, but a very crucial importance towards clinical applications will be played by the strategy for MENPs delivery. A high number of factors will influence the MENPs correct positioning, such as the efficiency of the delivery, as well as the long-term lasting of the MENPs in the desired location. This makes the choice of the positioning strategy and of the quantity of MENPs to be inserted highly complex. Even if preliminary experimental studies [19], [20] showed very promising in-vivo results, deep investigations by experimental in-vivo and multi-scale computational modelling studies will be required to obtain reliable estimation of the better strategies to be applied for DBS mediated by MENPs in human beings. Once optimized these aspects, the use of MENPs could offer a great step ahead in generating optimal therapy without triggering side effects. This characteristic, along with the minimally invasiveness, represent an important step ahead towards the possibility of developing a completely new paradigm for the stimulation of deep neural structures [20], [48], [49].

V. CONCLUSION

A computational approach was used to quantify the distributions of the electric field and electric potential induced by $CoFe_2O_4$-$BaTiO_3$ MENPs localized in the deep brain structures in a highly detailed anatomical head model, and by numerically comparing them to the distributions obtained by conventional DBS monopolar and bipolar electrode configurations. Results showed that very focused patterns of nervous fibers activation could be achieved, potentially minimizing side effects. These results, along with their minimally invasiveness nature and their proven biocompatibility, makes MENPs mediated DBS representing a significant improvement towards a minimally invasive strategy for stimulation of deep neural tissues.

ACKNOWLEDGMENT

The authors wish to thank ZMT Zurich MedTech AG (www.zmt.swiss) for providing SIM4Life software. *(Emma Chiaramello and Serena Fiocchi contributed equally to this work.)*

REFERENCES

[1] G. Deuschl et al., "A randomized trial of deep-brain stimulation for Parkinson's disease," *New England J. Med.*, vol. 355, no. 9, pp. 896–908, 2006.

[2] A. L. Benabid, P. Pollak, D. Gao, D. Hoffmann, P. Limousin, E. Gay, I. Payen, and A. Benazzouz, "Chronic electrical stimulation of the ventralis intermedius nucleus of the thalamus as a treatment of movement disorders," *J. Neurosurgery*, vol. 84, no. 2, pp. 203–214, Feb. 1996.

[3] M. J. Morrell, "Responsive cortical stimulation for the treatment of medically intractable partial epilepsy," *Neurology*, vol. 77, no. 13, pp. 1295–1304, 2011.

[4] V. Salanova et al., "Long-term efficacy and safety of thalamic stimulation for drug-resistant partial epilepsy," *Neurology*, vol. 84, no. 10, pp. 1017–1025, 2015.

[5] C. C. McIntyre, S. Miocinovic, and C. R. Butson, "Computational analysis of deep brain stimulation," *Exp. Rev. Med. Devices*, vol. 4, no. 5, pp. 615–622, 2007.
[6] A. Amon and F. Alesch, "Systems for deep brain stimulation: Review of technical features," *J. Neural Transmiss.*, vol. 124, no. 9, pp. 1083–1091, 2017.
[7] S. Hemm and K. Wårdell, "Stereotactic implantation of deep brain stimulation electrodes: A review of technical systems, methods and emerging tools," *Med. Biol. Eng. Comput.*, vol. 48, no. 7, pp. 611–624, 2010.
[8] J. N. Petry-Schmelzer et al., "Non-motor outcomes depend on location of neurostimulation in Parkinson's disease," *Brain*, vol. 142, no. 11, pp. 3592–3604, 2019.
[9] C. C. McIntyre, S. Mori, D. L. Sherman, N. V. Thakor, and J. L. Vitek, "Electric field and stimulating influence generated by deep brain stimulation of the subthalamic nucleus," *Clin. Neurophysiol.*, vol. 115, no. 3, pp. 589–595, Mar. 2004.
[10] A. M. M. Kuncel and W. Grill, "Selection of stimulus parameters for deep brain stimulation," *Clin. Neurophysiol.*, vol. 115, no. 11, pp. 2431–2441, 2004.
[11] C. R. Butson, S. E. Cooper, J. M. Henderson, and C. C. McIntyre, "Patient-specific analysis of the volume of tissue activated during deep brain stimulation," *NeuroImage*, vol. 34, no. 2, pp. 661–670, Jan. 2007.
[12] S. Miocinovic, "Computational analysis of subthalamic nucleus and lenticular fasciculus activation during therapeutic deep brain stimulation," *J. Neurophysiol.*, vol. 96, no. 3, pp. 1569–1580, 2006.
[13] J. E. Hoover and P. L. Strick, "Multiple output channels in the basal ganglia," *Science*, vol. 259, pp. 819–821, Feb. 1993.
[14] A. J. Bullard, B. C. Hutchison, J. Lee, C. A. Chestek, and P. G. Patil, "Estimating risk for future intracranial, fully implanted, modular neuroprosthetic systems: A systematic review of hardware complications in clinical deep brain stimulation and experimental human intracortical arrays," *Neuromodulation, Technol. Neural Interface*, vol. 23, no. 4, pp. 411–426, Jun. 2020.
[15] A. Frank, J. Bendig, I. Schniewind, W. H. Polanski, S. B. Sobottka, H. Reichmann, K. Akgün, T. Ziemssen, L. Klingelhoefer, and B. H. Falkenburger, "Serum neurofilament indicates that DBS surgery can cause neuronal damage whereas stimulation itself does not," *Sci. Rep.*, vol. 12, no. 1, pp. 1–5, Jan. 2022.
[16] D. Dominguez-Paredes, A. Jahanshahi, and K. L. Kozielski, "Translational considerations for the design of untethered nanomaterials in human neural stimulation," *Brain Stimulation*, vol. 14, no. 5, pp. 1285–1297, Sep. 2021.
[17] E. Gharibshahi, B. D. Young, A. S. Bhalla, and R. Guo, "Modeling, simulation and synthesis of multiferroic magnetoelectric $CoFe_2O_4/BaTiO_3$ composite nanoparticles," *Solid State Commun.*, vol. 333, Jul. 2021, Art. no. 114288.
[18] A. Singer, S. Dutta, E. Lewis, Z. Chen, J. C. Chen, N. Verma, B. Avants, A. K. Feldman, J. O'Malley, M. Beierlein, and C. Kemere, "Magnetoelectric materials for miniature, wireless neural stimulation at therapeutic frequencies," *Neuron*, vol. 107, no. 4, pp. 631–643, 2020.
[19] K. L. Kozielski, A. Jahanshahi, H. B. Gilbert, Y. Yu, Ö. Erin, D. Francisco, F. Alosaimi, Y. Temel, and M. Sitti, "Nonresonant powering of injectable nanoelectrodes enables wireless deep brain stimulation in freely moving mice," *Sci. Adv.*, vol. 7, no. 3, Jan. 2021, Art. no. eabc4189.
[20] T. Nguyen, J. Gao, P. Wang, A. Nagesetti, P. Andrews, S. Masood, Z. Vriesman, P. Liang, S. Khizroev, and X. Jin, "In vivo wireless brain stimulation via non-invasive and targeted delivery of magnetoelectric nanoparticles," *Neurotherapeutics*, vol. 18, no. 3, pp. 2091–2106, 2021.
[21] S. Khizroev, "Technobiology's enabler: The magnetoelectric nanoparticle," *Cold Spring Harbor Perspect. Med.*, vol. 9, no. 8, Aug. 2019, Art. no. a034207.
[22] K. Yue, R. Guduru, J. Hong, P. Liang, M. Nair, and S. Khizroev, "Magnetoelectric nano-particles for non-invasive brain stimulation," *PloS One*, vol. 7, Sep. 2012, Art. no. e44040.
[23] R. Guduru, "Magnetoelectric 'spin' on stimulating the brain," *Nanomedicine*, vol. 10, pp. 2051–2061, May 2015, doi: 10.2217/nnm.15.52.
[24] S. Fiocchi, E. Chiaramello, A. Marrella, M. Bonato, M. Parazzini, and P. Ravazzani, "Modelling of magnetoelectric nanoparticles as a key technology enabler for non-invasive brain stimulation," *J. Neural Eng.*, vol. 19, no. 5, p. 056020, Sep. 2022.
[25] A. Paffi, F. Apollonio, M. G. Puxeddu, M. Parazzini, G. D'Inzeo, P. Ravazzani, and M. Liberti, "A numerical study to compare stimulations by intraoperative microelectrodes and chronic macroelectrodes in the DBS technique," *BioMed Res. Int.*, vol. 2013, pp. 1–7, Oct. 2013.
[26] G. Duffley, D. N. Anderson, J. Vorwerk, A. D. Dorval, and C. R. Butson, "Evaluation of methodologies for computing the deep brain stimulation volume of tissue activated," *J. Neural Eng.*, vol. 16, no. 6, 2019, Art. no. 066024.
[27] S. Zhang, M. Tagliati, N. Pouratian, B. Cheeran, E. Ross, and E. Pereira, "Steering the volume of tissue activated with a directional deep brain stimulation lead in the Globus pallidus pars interna: A modeling study with heterogeneous," *Frontiers Comput. Neurosci.*, vol. 14, Sep. 2020, Art. no. 561180.
[28] M. I. Iacono, E. Neufeld, G. Bonmassar, E. Akinnagbe, A. Jakab, E. Cohen, N. Kuster, W. Kainz, and L. M. Angelone, "A computational model for bipolar deep brain stimulation of the subthalamic nucleus," in *Proc. 36th Annu. Int. Conf. IEEE Eng. Med. Biol. Soc.*, Aug. 2014, pp. 6258–6261.
[29] M. I. Iacono, E. Neufeld, E. Akinnagbe, K. Bower, J. Wolf, I. V. Oikonomidis, D. Sharma, B. Lloyd, B. J. Wilm, M. Wyss, K. P. Pruessmann, A. Jakab, N. Makris, E. D. Cohen, N. Kuster, W. Kainz, and L. M. Angelone, "MIDA: A multimodal imaging-based detailed anatomical model of the human head and neck," *PLoS One*, vol. 10, no. 4, Apr. 2015, Art. no. e0124126.
[30] A. Rabie, L. V. Metman, and K. V. Slavin, "Using 'functional' target coordinates of the subthalamic nucleus to assess the indirect and direct methods of the preoperative planning: Do the anatomical and functional targets coincide?" *Brain Sci.*, vol. 6, no. 4, p. 65, Dec. 2016.
[31] P. Novak, "Localization of the subthalamic nucleus in Parkinson disease using multiunit activity," *J. Neurol. Sci.*, vol. 310, nos. 1–2, pp. 44–49, 2011.
[32] J. Rong, Q. Wang, K. Liu, L. Tan, X. Ran, S. Zhang, Q. Li, and Y. Han, "A new atlas localization approach for subthalamic nucleus utilizing Chinese visible human head datasets," *PLoS one*, vol. 8, no. 2, Feb. 2013, Art. no. e57264.
[33] I. Mavridis, E. Boviatsis, and S. Anagnostopoulou, "Anatomy of the human subthalamic nucleus: A combined morphometric study," *Anatomy Res. Int.*, vol. 2013, pp. 1–8, Dec. 2013.
[34] E. O. Richter, T. Hoque, W. Halliday, A. M. Lozano, and J. A. Saint-Cyr, "Determining the position and size of the subthalamic nucleus based on magnetic resonance imaging results in patients with advanced Parkinson disease," *J. Neurosurg.*, vol. 100, no. 3, pp. 541–546, 2004.
[35] S. Betal, B. Shrestha, M. Dutta, L. F. Cotica, E. Khachatryan, K. Nash, L. Tang, A. S. Bhalla, and R. Guo, "Magneto-elasto-electroporation (MEEP): In-vitro visualization and numerical characteristics," *Sci. Rep.*, vol. 6, no. 1, pp. 1–15, Oct. 2016.
[36] S. Fiocchi, E. Chiaramello, A. Marrella, G. Suarato, M. Bonato, M. Parazzini, and P. Ravazzani, "Modeling of core-shell magneto-electric nanoparticles for biomedical applications: Effect of composition, dimension, and magnetic field features on magnetoelectric response," *PLoS One*, vol. 17, no. 9, Sep. 2022, Art. no. e0274676, doi: 10.1371/journal.pone.0274676.
[37] J. Malmivuo and R. Plonsey, *Bioelectromagnetism: Principles and Applications of Bioelectric and Biomagnetic Fields*. New York, NY, USA: Oxford Univ. Press, 1995.
[38] C. R. Butson and C. C. McIntyre, "Tissue and electrode capacitance reduce neural activation volumes during deep brain stimulation," *Clin. Neurophysiol.*, vol. 116, no. 10, pp. 2490–2500, Oct. 2005.
[39] S. Zhang, P. Silburn, N. Pouratian, B. Cheeran, L. Venkatesan, A. Kent, and A. Schnitzler, "Comparing current steering technologies for directional deep brain stimulation using a computational model that incorporates heterogeneous tissue properties," *Neuromodulation, Technol. Neural Interface*, vol. 23, no. 4, pp. 469–477, Jun. 2020, doi: 10.1111/ner.13031.
[40] P. A. Hasgall, F. Di Gennaro, C. Baumgartner, E. Neufeld, B. Lloyd, M. C. Gosselin, D. Payne, A. Klingenböck, and N. Kuster, "IT'IS database for thermal and electromagnetic parameters of biological tissues," Version 4.1, Feb. 2022. [Online]. Available: https://itis.swiss/database, doi: 10.13099/VIP21000-04-1.
[41] C. C. McIntyre, A. G. Richardson, and W. M. Grill, "Modeling the excitability of mammalian nerve fibers: Influence of afterpotentials on the recovery cycle," *J. Neurophysiol.*, vol. 87, no. 2, pp. 995–1006, Feb. 2002, doi: 10.1152/jn.00353.2001.
[42] F. Alonso, D. Vogel, J. Johansson, K. Wårdell, and S. Hemm, "Electric field comparison between microelectrode recording and deep brain stimulation systems—A simulation study," *Brain Sci.*, vol. 8, no. 2, p. 28, Feb. 2018.

[43] V. Corral-Flores, D. Bueno-Baqués, and R. F. Ziolo, "Synthesis and characterization of novel $CoFe_2O_4$–$BaTiO_3$ multiferroic core–shell-type nanostructures," *Acta Mater.*, vol. 58, no. 3, pp. 764–769, Feb. 2010.
[44] M. Lu and S. Ueno, "Comparison of the induced fields using different coil configurations during deep transcranial magnetic stimulation," *PLoS One*, vol. 12, no. 6, 2017, Art. no. e0178422.
[45] C. C. McIntyre, M. Savasta, L. K.-L. Goff, and J. L. Vitek, "Uncovering the mechanism(s) of action of deep brain stimulation: Activation, inhibition, or both," *Clin. Neurophysiol.*, vol. 115, no. 6, pp. 1239–1248, Jun. 2004.
[46] M. Åström, E. Diczfalusy, H. Martens, and K. Wårdell, "Relationship between neural activation and electric field distribution during deep brain stimulation," *IEEE Trans. Biomed. Eng.*, vol. 62, no. 2, pp. 664–672, Feb. 2015.
[47] C. R. Butson and C. C. McIntyre, "Role of electrode design on the volume of tissue activated during deep brain stimulation," *J. Neural Eng.*, vol. 3, no. 1, pp. 1–8, Mar. 2006.
[48] M. Kujawska and A. Kaushik, "Exploring magneto-electric nanoparticles (MENPs): A platform for implanted deep brain stimulation," *Neural Regener. Res.*, vol. 18, no. 1, p. 129, 2023, doi: 10.4103/1673-5374.340411.
[49] S. Kopyl, R. Surmenev, M. Surmeneva, Y. Fetisov, and A. Kholkin, "Magnetoelectric effect: Principles and applications in biology and medicine—A review," *Mater. Today Bio*, vol. 13, no. 12, Sep. 2021, Art. no. 100149, doi: 10.1016/j.mtbio.2021.100149.

EMMA CHIARAMELLO (Member, IEEE) received the master's and Ph.D. degrees in biomedical engineering from the Politecnico di Torino, Torino, Italy, in 2009 and 2013, respectively.

She is currently a Research Scientist with the Institute of Electronics, Computer, and Telecommunication Engineering, National Research Council of Italy, Rome, Italy. Her research interests include the study of the interactions between EMF and biological systems, with both deterministic dosimetry based on computational electromagnetism methods and stochastic dosimetry based on surrogate modeling.

SERENA FIOCCHI received the master's degree in biomedical engineering and the Ph.D. degree in bioengineering from the Polytechnic University of Milan, Milan, Italy, in 2009 and 2014, respectively. She is currently a Research Scientist with the Institute of Electronics, Computer, and Telecommunication Engineering, National Research Council of Italy, Rome, Italy. Her research interests include the study of the computational modeling of non-invasive brain and spinal stimulation techniques, the design and the optimization of biomedical technologies based on electromagnetic fields (EMF) for diagnostic and therapeutic applications, and the computational modeling of the interactions between EMF and biological systems.

MARTA BONATO (Student Member, IEEE) received the master's degree in biomedical engineering and the Ph.D. degree in bioengineering from the Polytechnic of Milan, Milan, Italy, in 2017 and 2021, respectively. Since September 2017, she is with the Institute of Electronics, Computer, and Telecommunication Engineering, Consiglio Nazionale delle Ricerche, Rome, Italy, as a Research Fellow. Her research interests include the study of the interaction of electromagnetic fields (EMF) with biological systems and the study of possible effects of EMF on health with both deterministic and stochastic dosimetry.

ALESSANDRA MARRELLA received the M.Sc. degree in bioengineering from the University of Genoa, in 2014, and the Ph.D. degree in biotechnologies in translational medicine, in 2018. From 2016 to 2017, she was a Visiting Scientist at the Harvard-MIT Division of Health Sciences and Technology (HST), USA. Since July 2020, she has been a Researcher with the National Research Council of Italy (CNR-IEIIT). Her research interests include the development of engineered in vitro and in silico models of healthy and pathological tissues.

GIULIA SUARATO was born in Milan, Italy, in 1985. She received the B.S. and M.S. degrees in materials science and engineering from the Polytechnic University of Milan and the Ph.D. degree in materials science and engineering from Stony Brook University (State University of New York, New York, USA), with a thesis on functional nano-constructs for proteins and drugs delivery to various 2-D and 3-D tissue models. Until the end of 2021, she worked as a Postdoctoral Researcher at the Italian Institute of Technology, Genova, between the Smart Materials Group and the Translational Pharmacology Facility, working on the design of active, naturally-derived scaffolds for wound healing, tissue engineering, and pharmaceutical applications. Since December 2021, she has been a Researcher with the National Research Council of Italy in the Institute of Electronics, Information Engineering and Telecommunications (CNR-IEIIT), focusing on the study of cell-nanoparticle interactions. Her research interests include the development of functional biomaterials to instruct and dictate cell growth and tissue regeneration.

MARTA PARAZZINI (Member, IEEE) is currently a Research Scientist with the Institute of Electronics, Computer, and Telecommunication Engineering, Italian National Research Council, Rome, Italy. Her primary research interests include the study of the interactions of EMF with biological systems, deterministic and stochastic computational dosimetry, and the medical applications of EMF, in particular the techniques for noninvasive brain stimulation.

PAOLO RAVAZZANI (Member, IEEE) received the master's degree in electronic engineering and the Ph.D. degree in bioengineering from the Politecnico di Milano, Milan, Italy. He is currently the Director of Research with the Institute of Electronics, Computer, and Telecommunication Engineering, Consiglio Nazionale delle Ricerche, Rome, Italy. His main research interests include the exposure assessment of electromagnetic fields related to the study of the possible effects of electromagnetic fields on health and the biomedical applications of electromagnetic fields.

Open Access funding provided by 'Consiglio Nazionale delle Ricerche' within the CRUI CARE Agreement